Eur. Phys. J. Special Topics **227**, 2241–2261 (2019)

https://doi.org/10.1140/epjst/e2019-800105-y

THE EUROPEAN PHYSICAL JOURNAL SPECIAL TOPICS

Review

The pseudogap regime in the unitary Fermi gas

S. Jensen[1,a], C.N. Gilbreth[2,b,c], and Y. Alhassid[1,d]

[1] Center for Theoretical Physics, Sloane Physics Laboratory, Yale University, New Haven, CT 06520, USA
[2] Institute for Nuclear Theory, Box 351550, University of Washington, Seattle, WA 98195, USA

Received 25 June 2018 / Received in final form 14 December 2018
Published online 5 March 2019

Abstract. We discuss the pseudogap regime in the unitary Fermi gas (UFG), with a particular emphasis on the auxiliary-field quantum Monte Carlo (AFMC) approach. We discuss possible signatures of the pseudogap, review experimental results, and survey analytic and quantum Monte Carlo techniques before focusing on AFMC calculations in the canonical ensemble. For the latter method, we discuss results for the heat capacity, condensate fraction, energy-staggering pairing gap, and spin susceptibility, and compare to experiment and results of other theoretical methods.

1 Introduction

The unitary Fermi gas (UFG) describes a system of spin-1/2 fermions interacting through a short-range interaction tuned to the limit of infinite scattering length. It is a strongly interacting many-particle system with connections to high-T_c superconductivity [1–3], quark matter [4], QCD plasmas [5], and neutron stars [6]. The UFG exhibits a superfluid phase transition with a high critical temperature T_c in units of the Fermi temperature T_F.

The UFG sits midway in the BCS-BEC crossover, the continuous transition between Fermi and Bose gases obtained by varying the parameter $(k_F a)^{-1}$, where a is the s-wave scattering length and k_F is the Fermi wavenumber. The Bardeen-Cooper-Schrieffer (BCS) regime, obtained for $(k_F a)^{-1} \sim -\infty$, is well-described by the BCS theory of Cooper pairs at temperatures below the superfluid critical temperature T_c, and by Fermi liquid theory for temperatures above but close to T_c. The Bose-Einstein condensate (BEC) regime, corresponding to $(k_F a)^{-1} \sim +\infty$, consists of a weakly interacting Bose gas of tightly bound dimers with binding energy $E = -\hbar^2/(ma^2)$. In the unitary limit $(k_F a)^{-1} = 0$, the two-body bound state in vacuum becomes a zero-energy resonance and the s-wave scattering cross section in vacuum is maximized. The BCS-BEC crossover has been realized experimentally

[a] e-mail: scott.jensen@yale.edu
[b] e-mail: christopher.gilbreth@gmail.com
[c] *Current address*: Department of Physics, Central Washington University, Ellensburg, WA 98926, USA.
[d] e-mail: yoram.alhassid@yale.edu

with ultracold atomic Fermi gases of ^{6}Li and ^{40}K near broad Feshbach resonances (for reviews see Refs. [7,8]).

The UFG is highly non-perturbative and presents a major challenge to theorists. It undergoes a phase transition to a superfluid below a certain critical temperature T_c. However, the nature of the UFG above T_c is still not completely understood, and of particular interest is the possible existence of a pseudogap regime, in which pairing correlations persist above the superfluid critical temperature. A pseudogap regime is known to exist in high-T_c superconductors (e.g., the underdoped cuprates), but its exact mechanism has eluded a precise theoretical description [3,9,10]. The difficulty in understanding the pseudogap regime in these high-T_c superconductors provides a strong motivation for understanding pairing correlations above T_c within the simpler context of the UFG, in which pseudogap effects can occur via preformed pairs [3]. The possible existence and extent of a pseudogap regime in the UFG has generated considerable debate [11]. Resolving this from a theoretical perspective requires precise theoretical calculations with controllable errors.

In this brief review, we discuss important theoretical and experimental results related to the pseudogap regime in the UFG, with a focus on our own recent quantum Monte Carlo simulations [12]. Pseudogap physics in the UFG has also been discussed in references [11,13,14].

This review is organized as follows. In Section 2, we introduce the UFG and the continuum and lattice models used to study this system. In Section 3, we discuss possible signatures of the pseudogap regime in the UFG. In Section 4, we review landmark experimental results. In Section 5 we present an overview of theoretical approaches, emphasizing results related to the pseudogap regime. In Section 6, we discuss recent canonical-ensemble quantum Monte Carlo simulations and their implications for the pseudogap. In Section 7, we conclude and discuss future prospects.

2 Unitary Fermi gas

2.1 Scattering amplitude and the unitary limit

Neutral cold atomic gases interact at large distances via the van der Waals interaction $V = -C/r^6$, which is effectively a short-range interaction. At low temperatures and densities, their scattering properties are well described by the low-momentum s-wave expansion for the scattering amplitude

$$f(k) = \frac{1}{-1/a - ik + r_e k^2/2 + \cdots}, \tag{1}$$

where a is the s-wave scattering length, r_e is the effective range, and $\cdots$ denotes higher-order corrections in the relative momentum $\hbar k$. This expansion is justified for neutral cold atomic interactions in the limits $r_0 \ll 1/k_F, \lambda_T$ where r_0 is the interaction range and $\lambda_T = (2\pi\hbar^2/mk_BT)^{1/2}$ is the thermal de Broglie wavelength. Here $k_F = (3\pi^2\rho)^{1/3}$ is the Fermi wavenumber for particle density ρ, and k_B is the Boltzmann constant. For a broad Feshbach resonance, the effective range parameter r_e is of the same order as r_0 [15].

The cross section $4\pi|f(k)|^2$ that corresponds to the scattering amplitude in (1) is maximized in the limit of infinite scattering length a and vanishing effective range r_e. This is the unitary limit, characterized more precisely by the conditions $k_Fa \to \infty$ and $r_e \ll 1/k_F, \lambda_T$.

2.2 Continuum model

In the vicinity of a broad Feshbach resonance, the lowest two atomic hyperfine states of the atoms can be modeled by two spin-1/2 states that interact via a contact interaction. The Hamiltonian of this system can be written as

$$\hat{H} = -\sum_{\sigma} \int d^3\mathbf{r}\hat{\psi}^{\dagger}_{\sigma}(\mathbf{r})\frac{\hbar^2\nabla^2}{2m}\hat{\psi}_{\sigma}(\mathbf{r}) + \int d^3\mathbf{r}\hat{\psi}^{\dagger}_{\uparrow}(\mathbf{r})\hat{\psi}^{\dagger}_{\downarrow}(\mathbf{r}')V(\mathbf{r}-\mathbf{r}')\hat{\psi}_{\downarrow}(\mathbf{r}')\hat{\psi}_{\uparrow}(\mathbf{r}), \quad (2)$$

where $\hat{\psi}^{\dagger}_{\sigma}(\mathbf{r})$ $[\hat{\psi}_{\sigma}(\mathbf{r})]$ creates (annihilates) a fermion at position $\mathbf{r}$ with spin σ, and obeys anti-commutation relations $\{\hat{\psi}_{\sigma}(\mathbf{r}), \hat{\psi}^{\dagger}_{\sigma'}(\mathbf{r}')\} = \delta(\mathbf{r}-\mathbf{r}')\delta_{\sigma,\sigma'}$. An appropriate potential in coordinate space is the regularized pseudopotential $V(\mathbf{r}) = g\delta(\mathbf{r})\frac{\partial}{\partial r}r$, with $g = 4\pi\hbar^2 a/m$ [8,16]. One can also use a regularized contact interaction $V(\mathbf{r}-\mathbf{r}') = V_0\delta(\mathbf{r}-\mathbf{r}')$ with a bare coupling V_0 chosen to produce the desired two-body scattering length. V_0 is determined from the Lippmann-Schwinger equation, leading to

$$\frac{1}{V_0} = \frac{m}{4\pi\hbar^2 a} - \int^{\Lambda} \frac{d^3k}{(2\pi)^3 2\epsilon_k} \quad (3)$$

with hard ultraviolet momentum cutoff $\hbar\Lambda$. Equation (2) with a contact interaction is the most frequently used model in theoretical studies of the UFG pseudogap.

2.3 Lattice model

The Hamiltonian (2) for a uniform gas can be modeled with N particles on a cubic lattice with $M = N_L^3$ lattice sites (the filling factor is defined as $\nu = N/M$), lattice spacing δx, and periodic boundary conditions. The lattice Hamiltonian is given by

$$\hat{H} = \sum_{\mathbf{k},\sigma} \epsilon_{\mathbf{k}}\hat{a}^{\dagger}_{\mathbf{k},\sigma}\hat{a}_{\mathbf{k},\sigma} + g\sum_{\mathbf{x}} \hat{n}_{\mathbf{x},\uparrow}\hat{n}_{\mathbf{x},\downarrow}, \quad (4)$$

where the single-particle dispersion relation is usually taken to be either quadratic $\epsilon_{\mathbf{k}} = \hbar^2\mathbf{k}^2/2m$ or of the tight-binding form $\epsilon_{\mathbf{k}} = \frac{\hbar^2}{m\delta x^2}\sum_{i=1}^{3}[1-\cos(k_i\delta x)]$ (where i labels the quasi-momentum components), and $g = V_0/(\delta x)^3$ is the lattice coupling. The operators $\hat{a}^{\dagger}_{\mathbf{k},\sigma}$ and $\hat{a}_{\mathbf{k},\sigma}$ are, respectively, creation and annihilation operators for a single-particle state with wavevector $\mathbf{k}$ and spin $\sigma = \pm 1/2$, and $\hat{n}_{\mathbf{x},\sigma} = \hat{\psi}^{\dagger}_{\mathbf{x},\sigma}\hat{\psi}_{\mathbf{x},\sigma}$ are on-site number operators. The lattice site creation and annihilation operators $\hat{\psi}^{\dagger}_{\mathbf{x},\sigma}, \hat{\psi}_{\mathbf{x},\sigma}$ obey the anti-commutation relations $\{\hat{\psi}_{\mathbf{x},\sigma}, \hat{\psi}^{\dagger}_{\mathbf{x}',\sigma'}\} = \delta_{\mathbf{x},\mathbf{x}'}\delta_{\sigma,\sigma'}$. Note that on a lattice the Dirac delta function $\delta(\mathbf{r}-\mathbf{r}')$ of the continuum model becomes the Kronecker delta function $\delta_{\mathbf{x},\mathbf{x}'}$.

As discussed in references [12,17], the single-particle model space should include all states within the complete first Brillouin zone, described by a cube in momentum space $|k_i| \leq \Lambda$ $(i = x, y, z)$ with $\Lambda = \pi/\delta x$. The bare coupling constant V_0 is chosen to reproduce the two-particle scattering length as in equation (3), where the integration region corresponds to the complete first Brillouin zone. The UFG is reproduced from the lattice model in the continuum limit $\nu \to 0$ and thermodynamic limit $N \to \infty$.

Exact results on the lattice are available for the three-body problem [18].

2.4 Trapped gases

Trapped gases can be described by equation (2) with the addition of a one-body trapping potential $V_{\rm trap}(r)$. An isotropically trapped system with $V_{\rm trap}(r) = m\omega^2 r^2/2$ was considered in reference [19]. A natural single-particle basis is given by the eigenstates $|n, l, m_l\rangle$ of the single-particle Hamiltonian $\hat{h}_0 = -\frac{\hbar^2}{2m}\nabla^2 + V_{\rm trap}$, where n is the radial quantum number, l is the orbital angular momentum, and m_l the magnetic quantum number, with energy $\epsilon_{nl} = (2n + l + 3/2)\hbar\omega$. One can truncate the single-particle basis to a total of $N_{\rm max}$ quanta of energy, i.e., $2n + l \leq N_{\rm max}$. An effective interaction was developed for trapped systems with fast convergence in a regularization parameter [20,21], but it does not have a good Monte Carlo sign. We consider only a contact interaction $V(\mathbf{r} - \mathbf{r}') = V_0\delta(\mathbf{r} - \mathbf{r}')$, with V_0 tuned to reproduce the two-particle ground-state energy as calculated in reference [16]. We note this regularization is only approximate, the methods of references [20–22] being more rigorous. This interaction was also used in reference [23].

3 Signatures of a pseudogap

Different observables have been proposed as signatures of a pseudogap regime, and there is no one definition which is universally accepted. Most often, the pseudogap regime refers to a depression in the single-particle density of states $\rho(\omega)$ at the chemical potential μ for temperatures above T_c. The single-particle density of states is given by $\rho(\omega) = \int \frac{d^3k}{(2\pi)^3} A(\mathbf{k}, \omega)$, where $A(\mathbf{k}, \omega)$ is the spectral function.

3.1 Spectral function

The spectral function $A(\mathbf{k}, \omega)$ is given by the imaginary part of the retarded Green function $G^R(\mathbf{k}, \omega)$ through the relation $A(\mathbf{k}, \omega) = -\pi^{-1}\mathrm{Im}[G^R(\mathbf{k}, \omega)]$. In BCS theory, it has the two-peak structure [24,25]

$$A(\mathbf{k}, \omega) = u_{\mathbf{k}}^2 \delta(\omega - E_{\mathbf{k}}^{(+)}) + v_{\mathbf{k}}^2 \delta(\omega - E_{\mathbf{k}}^{(-)}), \tag{5}$$

where $E_{\mathbf{k}}^{(\pm)} = \mu \pm E_{\mathbf{k}}$ and $E_{\mathbf{k}} = \sqrt{(\epsilon_{\mathbf{k}} - \mu)^2 + \Delta^2}$ is the quasiparticle energy (Δ is the excitation gap and $\epsilon_{\mathbf{k}} = \frac{\hbar^2\mathbf{k}^2}{2m}$). The amplitudes $u_{\mathbf{k}}, v_{\mathbf{k}}$ define the quasiparticle creation operators $\hat{\alpha}_{\mathbf{k}\uparrow}^\dagger = u_{\mathbf{k}}\hat{a}_{\mathbf{k}\uparrow}^\dagger - v_{\mathbf{k}}\hat{a}_{-\mathbf{k}\downarrow}$ and $\hat{\alpha}_{-\mathbf{k}\downarrow}^\dagger = u_{\mathbf{k}}\hat{a}_{-\mathbf{k}\downarrow}^\dagger + v_{\mathbf{k}}\hat{a}_{\mathbf{k}\uparrow}$ with $|u_{\mathbf{k}}|^2 + |v_{\mathbf{k}}|^2 = 1$. In a strongly correlated system, which cannot be well described by mean-field theory, $A(\mathbf{k}, \omega)$ will have a more complex form with broadened peaks. However, these broadened peaks can sometimes be fit to a modified quasiparticle dispersion [25,26]

$$E_{\mathbf{k}}^{(\pm)} = \mu \pm \sqrt{\left(\frac{m}{m^*}\epsilon_k + U - \mu\right)^2 + \Delta^2}\,. \tag{6}$$

Here m^* is the effective mass and U is a Hartree shift parameter. A nonzero Δ for $T > T_c$ indicates the existence of gapped quasiparticle excitations due to preformed pairs as in reference [26]. However, a more general signature of a pseudogap is a suppression of $A(\mathbf{k}, \omega)$ near the chemical potential $\omega = \mu$. The $E^{(-)}$ branch of (5) bends toward lower energies as the momentum is increased; this "backbending" is also sometimes cited as a signature of a pseudogap.

One can define a temperature scale T^* as the temperature at which signatures of pairing first appear as the temperature is lowered. Note that in general no phase transition occurs at T^*. In BCS theory, the onset of pairing and condensation occur simultaneously and $T^* = T_c$, where the gap parameter Δ is the order parameter describing the phase transition. In the BEC regime, however, the pairing temperature T^* is the temperature scale associated with the formation of dimers and is distinct from the much lower condensation temperature T_c of the dimers. For the UFG, the value of T^* ($T^* \geq T_c$) is still debated in the literature.

3.2 Thermodynamics

Several thermodynamic quantities have been studied for signatures of pseudogap effects.

3.2.1 Heat capacity

The heat capacity $C_V = (\partial E/\partial T)_V$ can be affected by pseudogap physics. Underdoped cuprate high-T_c superconductors, which display pseudogap effects, are seen to exhibit a suppression of $\gamma = C_V/T$ for $T > T_c$ [10], indicating deviation from Fermi liquid theory. On the other hand, it has been argued that in the UFG the specific heat should be enhanced above T_c (either relative to the BCS and BEC regimes, or by showing an upward trend as T approaches T_c from above) due to the existence of $T > T_c$ precursor pairing correlations [27,28]. The specific heat was measured across the superfluid phase transition in the UFG [29] (see Sect. 4).

3.2.2 Spin susceptibility

The uniform static spin susceptibility χ_s

$$\chi_s = \frac{1}{k_B T V} \langle (\hat{N}_\uparrow - \hat{N}_\downarrow)^2 \rangle \tag{7}$$

provides another interesting signature of pseudogap effects [1,2]. Pairing correlations tend to suppress χ_s as pair breaking excitations become energetically unfavorable. The spin susceptibility is therefore expected to drop below T^*, similar to the exponential suppression of the spin susceptibility for a BCS superfluid at low temperatures.

3.2.3 Pairing gap

A model-independent pairing gap can be defined from the staggering of the energy with particle number

$$\Delta_E = [2E(N/2-1, N/2) - E(N/2-1, N/2-1) - E(N/2, N/2)]/2\,, \tag{8}$$

where $E(N_1, N_2)$ denotes the energy of a system with N_1 spin-up and N_2 spin-down particles, and $N = N_1 + N_2$ is the total number of particles [8,30]. For attractive pairing one has $\Delta_E \geq 0$. This definition is used for atomic nuclei [31] at zero temperature. We expect the onset of such even-odd effects in the thermal energy to occur below a temperature for which pairs with a finite binding energy begin to form. In a

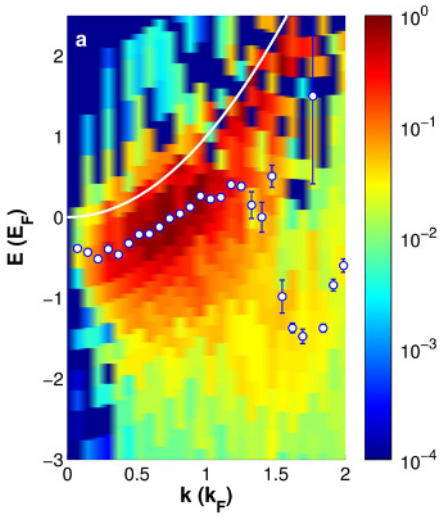

Fig. 1. Photoemission spectroscopy (PES) data [37] for the homogeneous Fermi gas near unitarity $[(k_F a)^{-1} = 0.1]$ at $T > T_c$. Color shows the normalized PES signal $I(p, E)$ (see text) as a function of the single-particle momentum p and energy E. The white line indicates the free particle dispersion $E \propto p^2$, and the circles are the peak positions. Adapted from the supplementary material of reference [37].

BCS superfluid this occurs below the critical temperature T_c, while in the UFG we expect this to occur below T^*.

The thermal energy $E(N_1, N_2)$ in equation (8) is defined in the canonical ensemble of fixed particle numbers N_1 and N_2. This canonical-ensemble formulation has been implemented in AFMC using particle-number projection [12,19] and reprojection [32]. For more details, see Section 6.

3.2.4 Equation of state

The equation of state has been studied in the normal phase and compared with predictions of Fermi liquid theory. In particular, the pressure of a Fermi liquid is expected to vary linearly with $(k_B T/\mu)^2$, when properly normalized. This has been investigated experimentally, as discussed in Section 4.

4 Experimental results

Effects of pairing correlations were observed in early spectroscopic measurements of trapped Fermi gases [33,34]. These experiments did not directly address pseudogap physics, but provided the first experimental evidence of pairing in the unitary regime.

The 2010 experiment of reference [35] appears to have been the first attempt to directly address pseudogap physics by measuring the spectral function of a trapped gas. A BCS-like dispersion, with backbending near k_F, was observed in photoemission spectra at temperatures above T_c. These results were subsequently analyzed in several papers with contradictory conclusions being drawn, one group describing a Fermi-liquid behavior [36], and another group explaining these results in terms of a pseudogap [27].

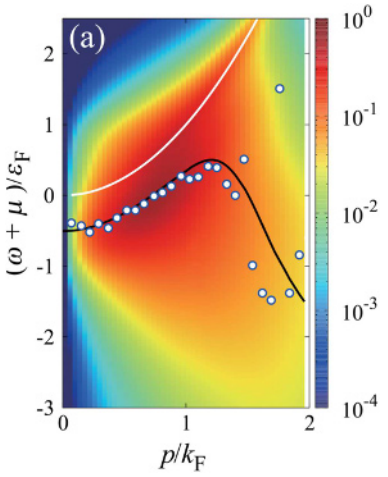

Fig. 2. Spectral intensity near unitarity $[(k_F a)^{-1} = 0.1]$ computed using a T-matrix approximation and compared with the experimental data in Figure 1. Color shows the computed intensity $I(p, E)$ (see text) including effects of the trap. The calculated peak position (black solid line) is compared to the experimental peak positions (white circles). Adapted from reference [38].

A more recent measurement accounted for trapping effects by focusing attention to the center of the cloud [37]. This experiment measured the photoemission spectral intensity $I(p, E) \propto p^2 A(p, E) f(E)$, where $f(E)$ is the Fermi-Dirac function and $A(p, E)$ is the single-particle spectral function. The result is shown in Figure 1 (normalized to $\int dp\, dE\, I(p, E) = 1$) near unitarity $[(k_F a)^{-1} = 0.1]$ and slightly above the critical temperature. The experimental data, including effects of finite resolution, is well-modeled by a fermionic quasiparticle spectral function plus an incoherent background thermal distribution of bound pairs. The weight of the quasiparticle signal decays to zero beyond $k_F a \approx 0.28$. The results of a T-matrix theory [38] (see Sect. 5.1) which display a pseudogap are shown in Figure 2 and compared with the experiment.

A measurement of the equation of state in 2010 found Fermi-liquid behavior of the pressure as a function of temperature [39]. The magnetic susceptibility in the normal phase was subsequently determined [36] and also shown to be consistent with a Fermi-liquid behavior. However, shortly afterward a measurement of the specific heat C_V across the superfluid phase transition [29] indicated non-Fermi-liquid behavior, in that C_V was not found to be linear in T in the normal phase. The same experiment also found a Fermi-liquid-like behavior in the pressure above T_c; see Figure 3.

5 Theoretical approaches

5.1 Strong-coupling theories

Early analytical approaches to the BCS-BEC crossover include those of Eagles [42] and Leggett [43], and Nozières and Schmidtt-Rink (NSR) [44]. NSR included pairing fluctuations to determine the dependence of T_c on the interaction strength. Reference [45] obtained similar NSR equations for T_c using Gaussian fluctuation theory.

Subsequently, various theories have emerged treating pairing correlations in the strong-coupling regime beyond the mean field by summing infinite series of certain diagrams in perturbation theory. A general difficulty with these theories is that they include uncontrolled approximations whose errors cannot be estimated a priori. The

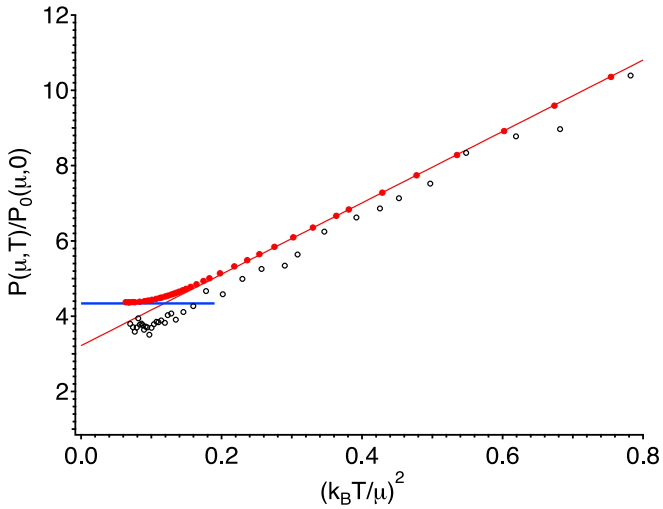

Fig. 3. Pressure of the homogeneous UFG as a function of $(k_{\mathrm{B}}T/\mu)^2$. The vertical axis shows the local pressure $P(\mu, T)$ of the trapped gas, normalized by the pressure $P_0(\mu, 0)$ of a non-interacting Fermi gas at zero temperature. The red solid circles are the experimental results of reference [29], the red line is a linear fit, and the solid blue line is the zero-temperature limit. Open circles are the earlier experimental results from reference [40]. The offset between the two experimental results is not fully understood but might be in part due to uncertainties in the Feshbach resonance position [41]. The linear behavior above $T \sim T_c$ is as expected for a Fermi liquid. Adapted from the supplemental material of reference [29].

two-species spin-balanced Fermi gas with contact interaction provides a useful testing ground for such theories, since it is experimentally accessible and permits quantum Monte Carlo simulations that are free of the sign problem (see Sects. 5.2 and 6).

A number of other theories addressing the pseudogap which we do not discuss here can be found in references [46–49].

5.1.1 Non-self-consistent T-matrix approaches

One of the earlier strong-coupling theories employed a non-self-consistent T-matrix approximation to describe the pseudogap in cold atomic Fermi gases [50]. Similar methods were applied in references [27,38,51–53]. In particular, the spectral function was calculated in references [27,51,53] at unitarity and compared to experiment in references [27,38]. It agrees well with the recent experiment of reference [37] (see Fig. 2). The T-matrix approximation of reference [50] predicts $T_c = 0.24\, T_F$ at unitarity, while an extended version used in references [54,55] predicts $T_c = 0.21\, T_F$ [55]. A recent development of this method can be found in reference [56].

Another approach, which describes a finite-temperature extension of the work of Leggett, is discussed in reference [57] and is referred to as the extended BCS-Leggett theory. In comparison with that of reference [50], it is less accurate in the BEC regime, but more accurate in the BCS regime. It yields $T_c = 0.26\, T_F$ at unitarity. References [57,58] provide detailed comparisons between the extended BCS-Leggett theory and the T-matrix approximations discussed above.

Figure 4 shows a comparison from reference [58] of the spectral function computed in the T-matrix approximation (left panel) and the extended BCS-Leggett theory (right panel), both at $T = 0.24\, T_F$, which is near T_c for these theories. Both theories

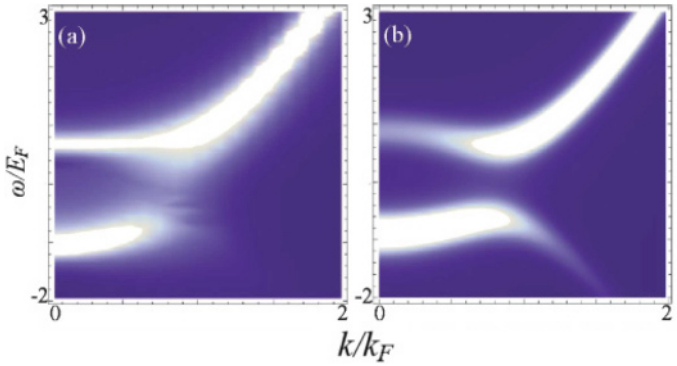

Fig. 4. Comparison of the spectral function $A(\mathbf{k}, \omega)$ of the UFG for two strong-coupling theories at $T = 0.24\,T_F$ (which is near T_c for these theories). The left panel shows a T-matrix approximation similar to reference [50], and the right panel is obtained in the extended BCS-Leggett theory. Adapted from reference [58].

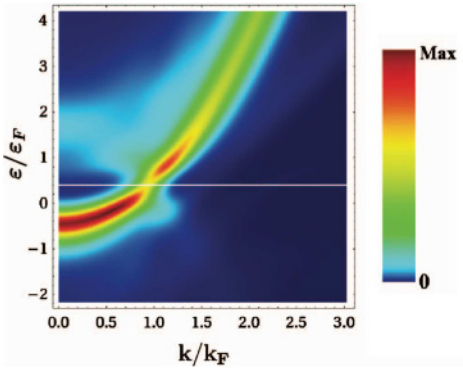

Fig. 5. Spectral function $A(\mathbf{k}, \omega)$ at unitarity for $T = T_c$ computed using a self-consistent Luttinger-Ward theory. At T_c, this theory shows only a weak two-branch structure. Adapted from reference [25].

show clear pseudogap effects, with the BCS-Leggett theory showing a more pronounced effect that includes backbending of the lower branch of the spectral function in addition to the two-peak structure.

5.1.2 Self-consistent Luttinger-Ward theory

A self-consistent theory was developed for the BCS-BEC crossover based on the Luttinger-Ward functional [25,59–62]. In this approach $T_c = 0.16(1)\,T_F$ at unitarity. When compared with other strong coupling theories, this value is closer to the experimental and quantum Monte Carlo values. Figure 5 shows the UFG spectral function calculated in this self-consistent approach at T_c. It exhibits only weak evidence of a pseudogap.

5.2 Quantum Monte Carlo methods

Several quantum Monte Carlo approaches have been used to study the UFG and its properties at finite temperature. There have also been a number of quantum Monte Carlo calculations of the UFG ground state ($T = 0$) studying the

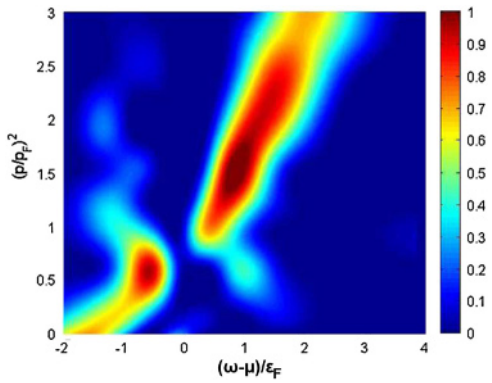

Fig. 6. Spectral function $A(\mathbf{k}, \omega)$ computed using AFMC at $T = 0.15\,T_F$ (the critical temperature reported by the authors of this work is $T_c \lesssim 0.15(1)\,T_F$ [63]). The horizontal axis is $(\omega - \mu)/\epsilon_F$ and the vertical axis is $(p/p_F)^2$, where μ is the chemical potential and p_F is the Fermi momentum. Adapted from reference [26].

Bertsch parameter [64,65], Tan's contact [66], the superfluid pairing gap [30,67], finite-size effects [68], and effective-range dependence [69–71]. Here we focus on finite-temperature approaches that are relevant to pseudogap phenomena.

5.2.1 Diagrammatic Monte Carlo methods

The diagrammatic quantum Monte Carlo approach stochastically samples the contributions of Feynman diagrams to correlation functions in the interaction picture. This has been implemented on a lattice and used to calculate thermodynamic properties of the normal and superfluid phases, extrapolating to the continuum and thermodynamic limits. In particular the critical temperature [72,73], and more recently the temperature dependence of the contact [74] have been computed and compared with experiment [75]. The lattice diagrammatic approach is described in detail in references [76,77].

The bold diagrammatic approach [78–81] works with fully dressed Green's functions directly in the continuum and thermodynamic limits. It was used to calculate the equation state of the UFG, in very good agreement with experiment. To date this method has been applied only above T_c.

5.2.2 Auxiliary-field Monte Carlo method

The auxiliary-field quantum Monte Carlo (AFMC) method [82,83] is based on the Hubbard-Stratonovich transformation [84,85], in which the thermal propagator $e^{-\beta \hat{H}}$ is written as a path integral of propagators of non-interacting particles in external auxiliary fields. The sum over the auxiliary-field configurations is then sampled stochastically. Finite-temperature lattice AFMC in the grand-canonical ensemble has been used to calculate both thermodynamic and dynamic properties of the UFG [26,63,86,87]. Unlike the diagrammatic methods, the computational cost of AFMC has so far prevented the extraction of observables in the full thermodynamic and continuum limits.

The spectral function has been computed for small lattices [26,86,87]. Figure 6 shows the result of reference [26] for $N = 50 - 55$ particles on a lattice of size 8^3 at $T = 0.15\,T_F$, which is essentially at their estimated critical temperature

$T_c \lesssim 0.15(1)\,T_F$. The result shows a clear gapped structure. The modified BCS dispersion in equation (6) was fitted to extract an effective gap parameter, giving $\Delta \approx 0.22\,\varepsilon_F$ at this temperature.

The static spin susceptibility was also computed [87] and seen to have substantial suppression for $T \geq T_c$, indicating a pseudogap regime where the pairing temperature scale is estimated to be $T^* = 0.20 - 0.25\,T_F$.

We note, however, that the calculations of references [26,63,86–88] used a spherical cutoff in the single-particle space $|\mathbf{k}| \leq \Lambda$ rather than the complete first Brillouin zone [see Eq. (4)]. As discussed in references [12,17], this approximation affects the two-particle scattering and does not reproduce the scattering properties of the UFG even in the continuum limit. See also Section 6.4.

5.2.3 Dynamical cluster Monte Carlo approach

The dynamical cluster quantum Monte Carlo approach [89–91] treats correlations on the lattice exactly for clusters of lattice sites up to a certain size, with longer-range correlations treated in a mean-field description. This approach has been applied to study the normal state spectral function with a lattice filling factor of $\nu = 0.3$ for several scattering lengths [92]. No clear pseudogap regime above the critical temperature was seen for the UFG.

6 Canonical-ensemble auxiliary-field quantum Monte Carlo methods

AFMC methods were developed in the canonical ensemble of fixed particle number for trapped Fermi gases of cold atoms using the CI shell model approach [19] and for uniform Fermi gases using a lattice formulation [12]. These approaches are inspired by AFMC methods developed for nuclei [93,94] in which the number of protons and neutrons are fixed; for reviews see references [95–97]. An advantage of the canonical ensemble is that it allows the model-independent calculation of a pairing gap from the staggering of the energy in particle number, equation (8). Canonical-ensemble quantum Monte Carlo calculations were also discussed in reference [98] and used to study finite-size effects in the Hubbard model. The direct implementation of particle-number projection is computationally intensive. In references [12,19] this technique was extensively optimized so it does not significantly increase the overall computation time.

For the lattice calculations of reference [12] we use the model of Section 2.3 with fixed numbers of $N_\uparrow$ and $N_\downarrow$ fermions on discrete lattices with lattice spacing δx and N_L points in each dimension (except when calculating the spin susceptibility χ_s, where only the total number of particles $N = N_\uparrow + N_\downarrow$ is fixed). We use the quadratic single-particle dispersion relation $\epsilon_{\mathbf{k}} = \hbar^2 k^2/2m$ and include all single-particle momentum states $\hbar\mathbf{k}$ within the first full Brillouin zone. For trapped gases, reference [19] used the model of Section 2.4 with fixed numbers of $N_\uparrow$ and $N_\downarrow$ fermions.

6.1 AFMC method

The AFMC method uses the representation of the thermal propagator $e^{-\beta\hat{H}}$ as a functional integral over auxiliary fields. We sketch below the derivation.

The Hamiltonian can be written in the form $\hat{H} = \hat{H}_0 + \hat{V}$, where $\hat{H}_0$ is a one-body operator and $\hat{V} = \sum_\alpha \lambda_\alpha \hat{O}_\alpha^2$ is the sum of squares of one-body operators $\hat{O}_\alpha$. In the

lattice case, $\hat{H}_0 = \hat{K} - g\hat{N}/2$, where $\hat{K}$ is the kinetic term, $\lambda_\alpha = g/2$, and $\hat{O}_\alpha$ are the on-site number operators $\hat{n}(\mathbf{x}) = \hat{n}_{\mathbf{x},\uparrow} + \hat{n}_{\mathbf{x},\downarrow}$. In the trapped case, the Hamiltonian can be decomposed in an angular-momentum-conserving formalism [19,95,99,100].

The propagator $e^{-\beta\hat{H}}$ is factorized using a Trotter decomposition $e^{-\beta\hat{H}} = (e^{-\Delta\beta\hat{H}})^{N_\tau}$, where we have divided the imaginary time β into N_τ time slices of length $\Delta\beta = \beta/N_\tau$. For each time slice, we use $e^{-\Delta\beta\hat{H}} = e^{-\Delta\beta\hat{H}_0/2}e^{-\Delta\beta\hat{V}}e^{-\Delta\beta\hat{H}_0/2} + O((\Delta\beta)^3)$ for our lattice calculations, and $e^{-\Delta\beta\hat{H}} = e^{-\Delta\beta\hat{H}_0}e^{-\Delta\beta\hat{V}} + O((\Delta\beta)^2)$ for our trapped calculations. The overall error is then $O((\Delta\beta)^2)$ or $O(\Delta\beta)$, respectively. Introducing an auxiliary field $\sigma_\alpha(\tau_n)$ for each $\hat{O}_\alpha$ and at each time slice n, we express $\exp(-\Delta\beta\lambda_\alpha\hat{O}_\alpha^2)$ as a Gaussian integral over $\sigma_\alpha(\tau_n)$ to obtain a discretized functional integral

$$e^{-\beta\hat{H}} \approx \int D[\sigma]G_\sigma\hat{U}_\sigma, \tag{9}$$

where $D[\sigma]$ is the integration measure and G_σ is a Gaussian weight. $\hat{U}_\sigma$ is the many-particle propagator $\hat{U}_\sigma = \hat{U}_{N_\tau}\cdots\hat{U}_1$, a time-ordered product in which each $\hat{U}_n$ is a product of exponentials of one-body operators.

The expectation value of an observable $\hat{O}$ can be written as a functional integral

$$\langle\hat{O}\rangle = \frac{\int D[\sigma]\langle\hat{O}\rangle_\sigma W_\sigma\Phi_\sigma}{\int D[\sigma]W_\sigma\Phi_\sigma}, \tag{10}$$

where $\langle\hat{O}\rangle_\sigma = \mathrm{Tr}(\hat{O}\hat{U}_\sigma)/\mathrm{Tr}(\hat{U}_\sigma)$ is the expectation value of $\hat{O}$ for a given auxiliary-field configuration σ, $W_\sigma = G_\sigma|\mathrm{Tr}(\hat{U}_\sigma)|$ is a positive-definite weight, and $\Phi_\sigma = \mathrm{Tr}(\hat{U}_\sigma)/|\mathrm{Tr}(\hat{U}_\sigma)|$ is the Monte Carlo sign. The high-dimensional integral in equation (10) is calculated by Monte Carlo sampling, for which we use the Metropolis-Hastings algorithm [101,102], updating one time slice at a time. The traces in the equations above are calculated in the canonical ensemble, as discussed in the next section.

The advantage the AFMC framework is that $\hat{U}_\sigma$ in equation (9) is a one-body propagator, so the expectation values of observables with respect to $\hat{U}_\sigma$ can be computed using matrix algebra in the single-particle space. In this single-particle space $\hat{U}_\sigma$ is represented by a chain of matrix products. For a large number of time slices, this product must be numerically stabilized [95]. This stabilization is achieved by a QDR decomposition: the matrix $\mathbf{U}_\sigma$ representing $\hat{U}_\sigma$ is stored in a decomposed form $\mathbf{U}_\sigma = QDR$ where Q is unitary, D is diagonal with positive entries, and R is unit upper triangular.

6.2 Particle-number projection

For each auxiliary-field configuration we project onto fixed particle number using a discrete Fourier transform [103], with projection operator

$$\hat{P}_{N_\sigma} = \frac{e^{-\beta\mu N_\sigma}}{M}\sum_{m=1}^{M} e^{-i\varphi_m N_\sigma}e^{(\beta\mu+i\varphi_m)\hat{N}_\sigma} \tag{11}$$

for $\sigma = \uparrow$ or $\downarrow$. Here $\varphi_m = \frac{2\pi m}{M}$ are quadrature points, $M = N_L^3$ is the number of lattice points (in the lattice case) or the number of single-particle harmonic oscillator

states (in the trapped case), and the chemical potential μ is introduced for numerical stability. The traces above are then evaluated in the canonical ensemble using $\mathrm{Tr}_{N_\uparrow,N_\downarrow}(\hat{X}) = \mathrm{Tr}_{\mathrm{GC}}(\hat{P}_{N_\uparrow}\hat{P}_{N_\downarrow}\hat{X})$ which allows us to write the canonical-ensemble trace as a sum of grand-canonical traces (with complex chemical potentials). The grand-canonical trace is calculated in the single-particle space for the one-body propagator $\hat{U}_\sigma$ using the relation

$$\mathrm{Tr}_{\mathrm{GC}}[e^{(\beta\mu+i\varphi_m)\hat{N}}\hat{U}_\sigma] = \det[\mathbb{1} + e^{(\beta\mu+i\varphi_m)}\mathbf{U}_\sigma] \,. \tag{12}$$

The canonical projection usually requires $O(M^4)$ operations to compute, particularly when combined with numerical stabilization. A canonical-ensemble algorithm allowing $O(M^3)$ scaling was introduced in references [19,104]. In the lattice calculations of reference [12], we have further reduced the computational time using several methods which effectively reduce the dimension of the single-particle model space for a given field configuration. In particular, the D factor of the decomposition $\mathbf{U}_\sigma = QDR$ contains information on the numerical scales in $\mathbf{U}_\sigma$, and can be used to truncate the model space by omitting the eigenspace of $\mathbf{U}_\sigma$ that corresponds to unoccupied states. At temperatures of interest this reduces the model space dimension to the order of a few hundreds and substantially speeds up the calculation of observables.

6.3 Canonical-ensemble observables

A number of observables were studied for a finite-size trapped Fermi gas [19] and for the uniform Fermi gas [12] to better understand their pairing correlations across the superfluid phase transition.

6.3.1 Condensate fraction and critical temperature

The condensate fraction describes the extent of off-diagonal long-range order (ODLRO) in the two-body density matrix $\rho_2(i\uparrow, j\downarrow; k\uparrow, l\downarrow) = \langle \hat{a}^\dagger_{i\uparrow}\hat{a}^\dagger_{j\downarrow}\hat{a}_{l\downarrow}\hat{a}_{k\uparrow}\rangle$ [105]. For the trapped gas the indices i, j, k, l refer to harmonic oscillator states, and for the uniform Fermi gas they refer to momentum states. When ODLRO is present, ρ_2 will acquire a maximal eigenvalue λ_2 which scales with the system size and corresponds to the occupation of a pair state. The value of λ_2 is bound by $[N(M-N/2+1)/(2M)] \leq N/2$, where M is the number of single-particle states ($M = N_L^3$ for a lattice). The condensate fraction can then be defined as $n = \langle\lambda_2\rangle/[N(M-N/2+1)/(2M)]$ or $n = \lambda_2/(N/2)$.

In Figure 7 we show the condensate fraction $n = \lambda_2/(N/2)$ for a finite-size trapped gas with $N = 20$ particles and for a maximal number of oscillator shells $N_{\max} = 11$, which is sufficient to reach convergence in $N_{\max}$ at $T = 0.125\,T_F$ [99]. For the trapped case $T_F = \epsilon_F = 4\hbar\omega$ (using units with $k_B = 1$). The condensate fraction begins to rise steeply below $T \approx 0.175\,T_F$, showing a signature of the superfluid phase transition, which in a finite-size system is more precisely a smooth crossover.

In Figure 8 we show the condensate fraction $n = \langle\lambda_2\rangle/[N(M-N/2+1)/(2M)]$ for the uniform gas with $N = 80, 130$ particles on $11^3, 13^3$ lattices, and compare to the experimental result of reference [29].

For the uniform gas we use finite-size scaling for the condensate fraction [72,73,106,107] to estimate the critical temperature. We find $T_c = 0.130(15)\;T_F$ at the finite filling factor $\nu \simeq 0.06$. This density corresponds to a sizable ratio of the effective range to the Fermi wavelength $k_F r_e \simeq 0.41$, where $r_e = 0.337\,\delta x$ for the lattice model we simulated [17]. The zero-density limit results of references [72,73] are given by

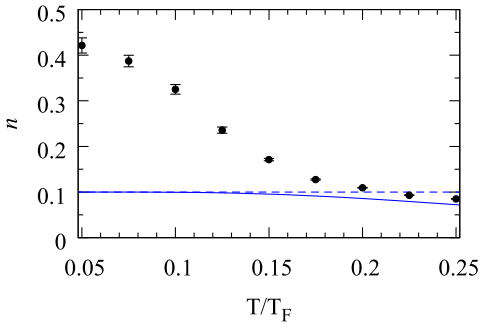

Fig. 7. Condensate fraction n for a trapped UFG with $N = 20$ particles as a function of T/T_F. The solid circles are the AFMC results, the solid line describes the noninteracting case, and the dashed line is the zero-temperature noninteracting limit $n = 2/N$. Adapted from reference [19].

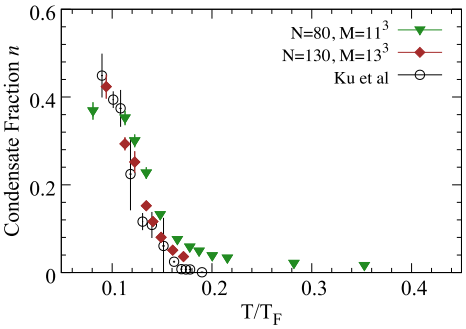

Fig. 8. Condensate fraction n for the uniform UFG vs. T/T_F. AFMC results [12] (solid symbols) are compared to the experimental result of reference [29] (open circles). The agreement between the experimental result and the $N = 130$ result is remarkable. We note, however, that our estimated critical temperature (for a filling factor of $\nu = 0.06$) $T_c \sim 0.13\,T_F$ is lower than the experimental $T_c = 0.167(13)T_F$ due to finite-range effects. Adapted from reference [12].

$T_c = 0.152(7)\,T_F$ and $T_c = 0.173(6)\,T_F$, respectively. Extrapolating to zero density using AFMC would be useful in future work to remove the finite-range contribution.

6.3.2 Heat capacity

The heat capacity calculations of references [12,19] are based on the method of reference [108], in which statistical errors are substantially reduced by using the same auxiliary-field configurations to compute $E(T + \Delta T)$ and $E(T - \Delta T)$ when calculating $(\partial E/\partial T)_V$ numerically, taking into account correlations in the statistical errors. In Figure 9, we show the result for the trapped case with 20 particles and $N_{\max} = 11$, for which C is converged at $T \leq 0.2\,T_F$. This heat capacity exhibits a clear signature of the superfluid phase transition.

In Figure 10 we show the result for the heat capacity of the uniform gas with $N = 40$ and $N = 80$ particles on lattices of size $M = 9^3$ and $M = 11^3$, respectively, and compare to experiment [29], the Luttinger-Ward result of references [109,110] (the data of Ref. [110] was used for the normal phase result), a non-self-consistent T-matrix calculation [27], and NSR theory [28]. The results of references [27,28] seem to differ significantly from the experimental data and from the AFMC results of reference [12]. However, we note that the agreement between these results and experiment is better

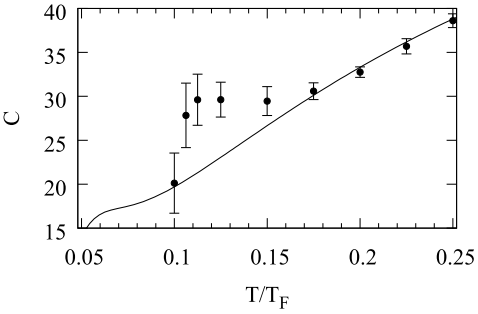

Fig. 9. Heat capacity for a trapped UFG with $N = 20$ particles as a function of T/T_F. Symbols and solid line are as in Figure 7. Adapted from reference [19].

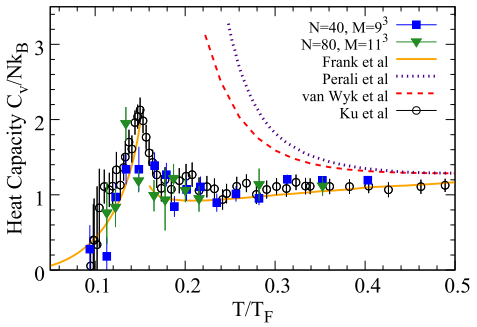

Fig. 10. AFMC heat capacity per particle for the UFG [12] (solid symbols) vs. T/T_F compared with the experiment of reference [29] (open circles) as well as the Luttinger-Ward result of references [109,110] (solid line), the T-matrix result of reference [27] (dotted line), and the NSR result of reference [28] (dashed line). Adapted from reference [12].

when plotted as a function of T/T_c, accounting for the differing values of T_c. The AFMC results of reference [12] agree well with experiment.

6.3.3 Pairing gap

The energy-staggering pairing gap Δ_E was computed in the canonical ensemble using equation (8) for both the trapped [19] and uniform [12] gases. Δ_E has the advantage of providing a model-independent signature of pairing correlations without the need for analytic continuation of Monte Carlo results.

In Figure 11 we show Δ_E for the trapped case for $N = 20$ and $N_{\max} = 9$; it is converged in $N_{\max}$ for $T \leq 0.2\ T_F$. The gap is slightly larger than zero at high temperatures due to finite-size effects. It begins to rapidly increase below $T \sim 0.175\ T_F$, the same temperature at which features in n and C appear, showing no evidence of a gap prior to condensation for this finite number of particles.

In Figure 12 we show Δ_E for the uniform UFG for $N = 40, 80, 130$ on lattices of size $M = 9^3, 11^3, 13^3$, respectively. We also show the $T = 0$ quantum Monte Carlo result of reference [67] and the low-temperature experimental result of reference [112]. These results are consistent with the spatially resolved radio-frequency spectroscopy result $\Delta_E/\varepsilon_F = 0.44(3)$ of reference [111]. The energy-staggering pairing gap Δ_E vanishes (or is very weak) for temperatures greater than the critical temperature $T_c \approx 0.13\ T_F$ which we estimate for the finite filling factor of $\nu = 0.06$.

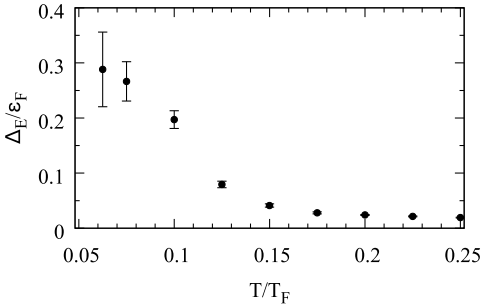

Fig. 11. Energy-staggering pairing gap Δ_E (in units of ε_F) for the trapped UFG with 20 particles vs. T/T_F, computed using canonical-ensemble AFMC. Adapted from reference [19].

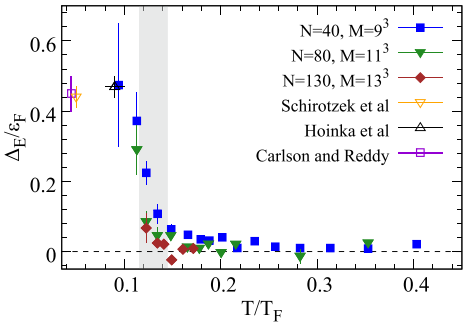

Fig. 12. Energy-staggering pairing gap Δ_E (in units of ε_F) for the uniform UFG vs. T/T_F using canonical-ensemble AFMC. The shaded vertical band shows our estimate of T_c calculated from the condensate fraction data using finite-size scaling. Also shown are the $T = 0$ quantum Monte Carlo result of reference [67] (open square), the experiment of reference [111] (open down triangle) and the recent experimental result of reference [112] (open up triangle). Adapted from reference [12].

6.3.4 Spin susceptibility

In Figure 13 we show our AFMC results for the spin susceptibility χ_s of the uniform gas in units of the zero-temperature free Fermi gas susceptibility $\chi_0 = 3\rho/2\varepsilon_F$ with particle density $\rho = \nu/(\delta x)^3$, along with several other theoretical results. For this observable we use a single particle-number projection onto the total number $N = N_\uparrow + N_\downarrow$ of particles. As discussed in Section 3, a decrease in the spin susceptibility is expected as the temperature is lowered below T^*. Comparing the temperature scale where this decrease occurs to the critical temperature T_c allows a determination of the pseudogap regime [2]. The strong-coupling calculations of references [55,113] are consistent with pseudogap physics, showing a "spin-gap" emerging via suppression in χ_s for $T > T_c$. The AFMC result of reference [87] also shows clear suppression in χ_s for temperatures below $\sim 0.25\, T_F$, a value significantly higher than the estimated $T_c \lesssim 0.15(1)\, T_F$ [63]. The result obtained in the self-consistent Luttinger-Ward theory of reference [62] does not show a clear signature of a pseudogap and is consistent with the spectral function result for $T = T_c$ shown in Figure 5. The calculation of reference [114], which uses an NSR-based approach, also shows no clear indication of a pseudogap or decrease in the spin susceptibility as the temperature is lowered.

Our results show a weak signature of a spin-gap above T_c. We observe a moderate decrease in the spin susceptibility for $N = 130$ particles below $T \approx 0.17\, T_F$, which is

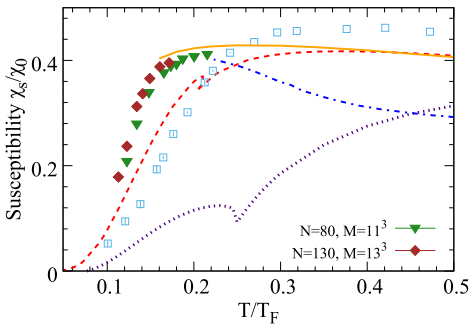

Fig. 13. Spin susceptibility χ_s for the uniform UFG computed using our canonical-ensemble AFMC (solid symbols), the AFMC result of reference [87] (open squares), the T-matrix result of reference [113] (dotted line), the T-matrix result of reference [55] (dashed line), the fully self-consistent Luttinger-Ward result of reference [62] (solid line), and the self-consistent NSR result of reference [114] (dashed-dotted line). Adapted from reference [12].

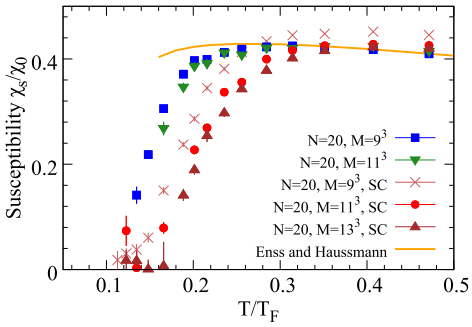

Fig. 14. Canonical-ensemble AFMC results for the spin susceptibility of $N = 20$ particles calculated with no cutoff on lattice sizes $9^3, 11^3$ and with a spherical cutoff (SC) on lattice sizes $9^3, 11^3, 13^3$. There is a substantial difference between the no cutoff and spherical cutoff results as the continuum is approached for lower filling factors. The solid line is the result of reference [62].

greater than our estimated T_c. However, while we estimated T_c in the thermodynamic limit for a filling factor $\nu = 0.06$ using finite-size scaling, no such thermodynamic limit has been taken with χ_s, and the trend for larger systems seems to indicate that the effect will be smaller in this limit.

6.4 Spherical cutoff

A spherical cutoff in the single-particle momentum of the uniform gas does not reproduce the two-particle scattering properties of the UFG even in the continuum limit [12,17]. The spin susceptibility provides a useful observable for testing the effects of a spherical cutoff on the many-particle physics. In Figure 14 we show the spin susceptibility for a fixed number $N = 20$ of particles on several lattice sizes, with and without a spherical cutoff in the single-particle momentum space. Even at the lowest filling factors studied, $\nu = 0.015, 0.009$ (corresponding, respectively, to lattice sizes of $11^3, 13^3$), the spherical cutoff effects survive and affect predictions for the value of T^* and pseudogap physics.

7 Conclusion

The nature of the UFG above the critical temperature T_c for superfluidity has attracted much interest, both theoretically and experimentally. Some of the measured observables are consistent with Fermi liquid behavior above T_c (e.g., the pressure, Fig. 3), while others are not (e.g., the spectral function observed in photoemission spectroscopy, Fig. 1). Results of theoretical calculations still vary considerably, with some predicting pronounced pseudogap effects and others not. In particular, the heat capacity in Figure 10 and the spin susceptibility in Figure 14 vary widely among different theories.

Measurements of the temperature dependence of the spin susceptibility and model-independent pairing gap would shed light on the pseudogap regime of the UFG. Past experiments have used trapped systems to infer the properties of the uniform gas, but an experimental setup of a uniform gas was recently reported [115]. Such experiments, expected in the near future, will address more directly the properties of the uniform gas and might provide better insight into pseudogap physics.

Quantum Monte Carlo methods have provided accurate calculations of the critical temperature and thermal energy, but results for the pseudogap are either less reliable or incomplete. Within the framework of AFMC, a reliable extrapolation for both the thermodynamic and continuum limits would be a very significant achievement, particularly if the spectral function could be computed using the full first Brillouin zone of the lattice. This would provide a benchmark for strong-coupling theories and other methods, such as the bold diagrammatic Monte Carlo, whose convergence properties are not well known. The canonical-ensemble AFMC calculations of reference [12] have made progress toward this goal by carefully fixing the filling factor, studying convergence, and computing new observables (the energy-staggering pairing gap and heat capacity). We have seen that it is important to take into account the complete first Brillouin zone of the lattice in momentum space. However, AFMC calculations on larger lattices are still computationally very challenging.

We thank N. Navon, G.F. Bertsch, and T. Enss for useful discussions. We also thank M.J.H. Ku for providing the experimental data of reference [29], and T. Enss, B. Frank, P. Magierski, Y. Ohashi, P. Pieri, G. C. Strinati, H. Tajima, M. Urban, G. Wlazłowski, and W. Zwerger for providing theoretical results shown in Figures 8, 10, 13, and 14. This work was supported in part by the U.S. DOE grants Nos. DE-FG02-91ER40608, DE-SC0019521, and DE-FG02-00ER41132. The research presented here used resources of the National Energy Research Scientific Computing Center, a DOE Office of Science User Facility supported by the Office of Science of the U.S. Department of Energy under Contract No. DE-AC02-05CH11231. We also thank the Yale Center for Research Computing for guidance and use of the research computing infrastructure.

Author contribution statement

S.J. and C.N.G. contributed to the AFMC calculations shown in Sections 6.3 and 6.4. All authors contributed to the writing of this brief review.

References

1. M. Randeria, N. Trivedi, A. Moreo, R.T. Scalettar, Phys. Rev. Lett. **69**, 2001 (1992)
2. N. Trivedi, M. Randeria, Phys. Rev. Lett. **75**, 312 (1995)
3. M. Randeria, Nat. Phys. **6**, 561 (2010)

4. Y. Nishida, H. Abuki, Phys. Rev. D **72**, 096004 (2005)
5. A. Adams, L.D. Carr, T. Schäfer, P. Steinberg, J.E. Thomas, N. J. Phys. **14**, 115009 (2012)
6. S. Gandolfi, A. Gezerlis, J. Carlson, Ann. Rev. Nucl. Particle Sci. **65**, 303 (2015)
7. I. Bloch, J. Dalibard, W. Zwerger, Rev. Mod. Phys. **80**, 885 (2008)
8. S. Giorgini, L.P. Pitaevskii, S. Stringari, Rev. Mod. Phys. **80**, 1215 (2008)
9. E. Dagotto, Rev. Mod. Phys. **66**, 763 (1994)
10. T. Timusk, B. Statt, Rep. Prog. Phys. **62**, 61 (1999)
11. E.J. Mueller, Rep. Prog. Phys. **80**, 104401 (2017)
12. S. Jensen, C.N. Gilbreth, Y. Alhassid, arXiv:1801.06163 (2018)
13. Q. Chen, J. Stajic, S. Tan, K. Levin, Phys. Rep. **412**, 1 (2005)
14. Q. Chen, J. Wang, Front. Phys. **9**, 539 (2014)
15. Y. Castin, F. Werner, The Unitary Gas and its Symmetry Properties, in *The BCS-BEC Crossover and the Unitary Fermi Gas*, edited by W. Zwerger (Springer-Verlag, Berlin, Heidelberg, 2012), pp. 127–191
16. T. Busch, B.G. Englert, K. Rzażewski, M. Wilkens, Found. Phys. **28**, 549 (1998)
17. F. Werner, Y. Castin, Phys. Rev. A **86**, 013626 (2012)
18. L. Pricoupenko, Y. Castin, J. Phys. A: Math. Theor. **40**, 12863 (2007)
19. C.N. Gilbreth, Y. Alhassid, Phys. Rev. A **88**, 063643 (2013)
20. Y. Alhassid, G.F. Bertsch, L. Fang, Phys. Rev. Lett. **100**, 230401 (2008)
21. C.N. Gilbreth, Y. Alhassid, Phys. Rev. A **85**, 033621 (2012)
22. I. Stetcu, B.R. Barrett, U. van Kolck, J.P. Vary, Phys. Rev. A **76**, 063613 (2007)
23. A. Mukherjee, Y. Alhassid, Phys. Rev. A **88**, 053622 (2013)
24. A. Fetter, J.D. Walecka, *Quantum theory of many-particle systems* (McGraw-Hill, 1971)
25. R. Haussmann, M. Punk, W. Zwerger, Phys. Rev. A **80**, 063612 (2009)
26. P. Magierski, G. Wlazłowski, A. Bulgac, J.E. Drut, Phys. Rev. Lett. **103**, 210403 (2009)
27. A. Perali, F. Palestini, P. Pieri, G.C. Strinati, J.T. Stewart, J.P. Gaebler, T.E. Drake, D.S. Jin, Phys. Rev. Lett. **106**, 060402 (2011)
28. P. van Wyk, H. Tajima, R. Hanai, Y. Ohashi, Phys. Rev. A **93**, 013621 (2016)
29. M.J.H. Ku, A.T. Sommer, L.W. Cheuk, M.W. Zwierlein, Science **335**, 563 (2012)
30. J. Carlson, S.Y. Chang, V.R. Pandharipande, K.E. Schmidt, Phys. Rev. Lett. **91**, 050401 (2003)
31. A. Bohr, B. Mottelson, in *Nuclear Structure* (Benjamin, Reading, Massachusetts, 1969), Vol. I
32. Y. Alhassid, S. Liu, H. Nakada, Phys. Rev. Lett. **83**, 4265 (1999)
33. C. Chin, M. Bartenstein, A. Altmeyer, S. Riedl, S. Jochim, J.H. Denschlag, R. Grimm, Science **305**, 1128 (2004)
34. M. Greiner, C.A. Regal, D.S. Jin, Phys. Rev. Lett. **94**, 070403 (2005)
35. J.P. Gaebler, J.T. Stewart, T.E. Drake, D.S. Jin, A. Perali, P. Pieri, G.C. Strinati, Nat. Phys. **6**, 569 (2010)
36. S. Nascimbène, N. Navon, S. Pilati, F. Chevy, S. Giorgini, A. Georges, C. Salomon, Phys. Rev. Lett. **106**, 215303 (2011)
37. Y. Sagi, T.E. Drake, R. Paudel, R. Chapurin, D.S. Jin, Phys. Rev. Lett. **114**, 075301 (2015)
38. M. Ota, H. Tajima, R. Hanai, D. Inotani, Y. Ohashi, Phys. Rev. A **95**, 053623 (2017)
39. N. Navon, S. Nascimbène, F. Chevy, C. Salomon, Science **328**, 729 (2010)
40. S. Nascimbène, N. Navon, K. Jiang, F. Chevy, C. Salomon, Nature **463**, 1057 (2010)
41. N. Navon, private communication (2018)
42. D.M. Eagles, Phys. Rev. **186**, 456 (1969)
43. A.J. Leggett, in *Modern trends in the theory of condensed matter* (Springer, 1980), pp. 13–27
44. P. Nozières, S. Schmitt-Rink, J. Low Temp. Phys. **59**, 195 (1985)
45. C.A.R. Sá de Melo, M. Randeria, J.R. Engelbrecht, Phys. Rev. Lett. **71**, 3202 (1993)
46. O. DeWolfe, O. Henriksson, C. Wu, Ann. Phys. **387**, 75 (2017)

47. K.B. Gubbels, H.T.C. Stoof, Phys. Rev. A **84**, 013610 (2011)
48. T. Debelhoir, N. Dupuis, Phys. Rev. A **93**, 023642 (2016)
49. E.V. Doggen, J.J. Kinnunen, Sci. Rep. **5**, 9539 (2015)
50. A. Perali, P. Pieri, G.C. Strinati, C. Castellani, Phys. Rev. B **66**, 024510 (2002)
51. S. Tsuchiya, R. Watanabe, Y. Ohashi, Phys. Rev. A **80**, 033613 (2009)
52. G.C. Strinati, Pairing Fluctuations Approach to the BCS–BEC Crossover, in *The BCS-BEC Crossover and the Unitary Fermi Gas*, edited by W. Zwerger (Springer-Verlag, Berlin, Heidelberg, 2012), pp. 99–126
53. M.D. Reichl, E.J. Mueller, Phys. Rev. A **91**, 043627 (2015)
54. T. Kashimura, R. Watanabe, Y. Ohashi, Phys. Rev. A **86**, 043622 (2012)
55. H. Tajima, T. Kashimura, R. Hanai, R. Watanabe, Y. Ohashi, Phys. Rev. A **89**, 033617 (2014)
56. L. Pisani, A. Perali, P. Pieri, G.C. Strinati, Phys. Rev. B **97**, 014528 (2018)
57. K. Levin, Q. Chen, C.C. Chien, Y. He, Ann. Phys. **325**, 233 (2010)
58. C.C. Chien, H. Guo, Y. He, K. Levin, Phys. Rev. A **81**, 023622 (2010)
59. R. Haussmann, Z. Phys. B: Condens. Matter **91**, 291 (1993)
60. R. Haussmann, Phys. Rev. B **49**, 12975 (1994)
61. R. Haussmann, W. Rantner, S. Cerrito, W. Zwerger, Phys. Rev. A **75**, 023610 (2007)
62. T. Enss, R. Haussmann, Phys. Rev. Lett. **109**, 195303 (2012)
63. A. Bulgac, J.E. Drut, P. Magierski, Phys. Rev. A **78**, 023625 (2008)
64. J. Carlson, S. Reddy, Phys. Rev. Lett. **95**, 060401 (2005)
65. J. Carlson, S. Gandolfi, K.E. Schmidt, S. Zhang, Phys. Rev. A **84**, 061602 (2011)
66. S. Gandolfi, K.E. Schmidt, J. Carlson, Phys. Rev. A **83**, 041601 (2011)
67. J. Carlson, S. Reddy, Phys. Rev. Lett. **100**, 150403 (2008)
68. M.M. Forbes, S. Gandolfi, A. Gezerlis, Phys. Rev. Lett. **106**, 235303 (2011)
69. X. Li, J.c.v. Kolorenč, L. Mitas, Phys. Rev. A **84**, 023615 (2011)
70. M.M. Forbes, S. Gandolfi, A. Gezerlis, Phys. Rev. A **86**, 053603 (2012)
71. L.M. Schonenberg, G.J. Conduit, Phys. Rev. A **95**, 013633 (2017)
72. E. Burovski, N. Prokof'ev, B. Svistunov, M. Troyer, Phys. Rev. Lett. **96**, 160402 (2006)
73. O. Goulko, M. Wingate, Phys. Rev. A **82**, 053621 (2010)
74. O. Goulko, M. Wingate, Phys. Rev. A **93**, 053604 (2016)
75. Y. Sagi, T.E. Drake, R. Paudel, D.S. Jin, Phys. Rev. Lett. **109**, 220402 (2012)
76. A.N. Rubtsov, V.V. Savkin, A.I. Lichtenstein, Phys. Rev. B **72**, 035122 (2005)
77. E. Burovski, N. Prokof'ev, B. Svistunov, M. Troyer, N. J. Phys. **8**, 153 (2006)
78. N. Prokof'ev, B. Svistunov, Phys. Rev. Lett. **99**, 250201 (2007)
79. N. Prokof'ev, B. Svistunov, Phys. Rev. B **77**, 020408 (2008)
80. K. Van Houcke, F. Werner, E. Kozik, N. Prokof'ev, B. Svistunov, M. Ku, A. Sommer, L. Cheuk, A. Schirotzek, M. Zwierlein, Nat. Phys. **8**, 366 (2012)
81. R. Rossi, T. Ohgoe, E. Kozik, N. Prokof'ev, B. Svistunov, K. Van Houcke, F. Werner, Phys. Rev. Lett. **121**, 130406 (2018)
82. R. Blankenbecler, D.J. Scalapino, R.L. Sugar, Phys. Rev. D **24**, 2278 (1981)
83. S.R. White, D.J. Scalapino, R.L. Sugar, E.Y. Loh, J.E. Gubernatis, R.T. Scalettar, Phys. Rev. B **40**, 506 (1989)
84. R.L. Stratonovich, Dokl. Akad. Nauk SSSR [Sov. Phys. - Dokl.] **115**, 1097 (1957)
85. J. Hubbard, Phys. Rev. Lett. **3**, 77 (1959)
86. P. Magierski, G. Wlazłowski, A. Bulgac, Phys. Rev. Lett. **107**, 145304 (2011)
87. G. Wlazłowski, P. Magierski, J.E. Drut, A. Bulgac, K.J. Roche, Phys. Rev. Lett. **110**, 090401 (2013)
88. A. Bulgac, J.E. Drut, P. Magierski, Phys. Rev. Lett. **96**, 090404 (2006)
89. M.H. Hettler, A.N. Tahvildar-Zadeh, M. Jarrell, T. Pruschke, H.R. Krishnamurthy, Phys. Rev. B **58**, R7475 (1998)
90. M.H. Hettler, M. Mukherjee, M. Jarrell, H.R. Krishnamurthy, Phys. Rev. B **61**, 12739 (2000)
91. T. Maier, M. Jarrell, T. Pruschke, M.H. Hettler, Rev. Mod. Phys. **77**, 1027 (2005)
92. S.Q. Su, D.E. Sheehy, J. Moreno, M. Jarrell, Phys. Rev. A **81**, 051604 (2010)

93. G.H. Lang, C.W. Johnson, S.E. Koonin, W.E. Ormand, Phys. Rev. C **48**, 1518 (1993)
94. Y. Alhassid, D.J. Dean, S.E. Koonin, G. Lang, W.E. Ormand, Phys. Rev. Lett. **72**, 613 (1994)
95. S. Koonin, D. Dean, K. Langanke, Phys. Rep. **278**, 1 (1997)
96. Y. Alhassid, Int. J. Mod. Phys. B **15**, 1447 (2001)
97. Y. Alhassid, Auxiliary-field quantum Monte Carlo methods in nuclei, in *Emergent Phenomena in Atomic Nuclei from Large-Scale Modeling: a Symmetry-Guided Perspective*, edited by K.D. Launey (World Scientific, Singapore, 2017), pp. 267–298
98. Z. Wang, F.F. Assaad, F. Parisen Toldin, Phys. Rev. E **96**, 042131 (2017)
99. C.N. Gilbreth, Ph.D. thesis, Yale University, 2013
100. C. Özen, N.T. Zinner, Eur. Phys. J. D **68**, 225 (2014)
101. N. Metropolis, A.W. Rosenbluth, M.N. Rosenbluth, A.H. Teller, E. Teller, J. Chem. Phys. **21**, 1087 (1953)
102. W.K. Hastings, Biometrika **57**, 97 (1970)
103. W.E. Ormand, D.J. Dean, C.W. Johnson, G.H. Lang, S.E. Koonin, Phys. Rev. C **49**, 1422 (1994)
104. C.N. Gilbreth, Y. Alhassid, Comput. Phys. Commun. **188**, 1 (2015)
105. C.N. Yang, Rev. Mod. Phys. **34**, 694 (1962)
106. K. Binder, Phys. Rev. Lett. **47**, 693 (1981)
107. N. Goldenfeld, *Lectures on phase transitions and the renormalization group* (Addison-Wesley, Advanced Book Program, Reading, Mass., 1992)
108. S. Liu, Y. Alhassid, Phys. Rev. Lett. **87**, 022501 (2001)
109. W. Zwerger, Strongly Interacting Fermi Gases, in *Proceedings of the International School of Physics "Enrico Fermi"- Course 191 "Quantum Matter at Ultralow Temperatures"*, edited by M. Inguscio, W. Ketterle, S. Stringari, G. Roati (IOS Press, Amsterdam, SIF Bologna, 2016), pp. 63–142
110. B. Frank, J. Lang, W. Zwerger, JETP **127**, 812 (2018)
111. A. Schirotzek, Y.I. Shin, C.H. Schunck, W. Ketterle, Phys. Rev. Lett. **101**, 140403 (2008)
112. S. Hoinka, P. Dyke, M.G. Lingham, J.J. Kinnunen, G.M. Bruun, C.J. Vale, Nat. Phys. **13**, 943 (2017)
113. F. Palestini, P. Pieri, G.C. Strinati, Phys. Rev. Lett. **108**, 080401 (2012)
114. P.A. Pantel, D. Davesne, M. Urban, Phys. Rev. A **90**, 053629 (2014)
115. B. Mukherjee, Z. Yan, P.B. Patel, Z. Hadzibabic, T. Yefsah, J. Struck, M.W. Zwierlein, Phys. Rev. Lett. **118**, 123401 (2017)